A quantum spin liquid candidate isolated in a two-dimensional $Co^{II}Rh^{III}$ bimetallic oxalate network

Enrique Burzurí,*[a,b,c] María José Martínez-Pérez,[d] Carlos Martí-Gastaldo,[e] Marco Evangelisti,[d] Samuel Mañas-Valero,[e] Eugenio Coronado,[e] Jesús I. Martínez,[d] Jose Ramon Galan-Mascaros[f,g] and Fernando Luis *[d]

[a.] *Departamento de Física de la Materia Condensada, Universidad Autónoma de Madrid, E-28049 Madrid, Spain*
[b.] *Condensed Matter Physics Center (IFIMAC) and Instituto Universitario de Ciencia de Materiales "Nicolás Cabrera" (INC), Universidad Autónoma de Madrid, E-28049 Madrid, Spain*
[c.] *IMDEA Nanociencia, C\Faraday 9, Ciudad Universitaria de Cantoblanco, Madrid, Spain.*
[d.] *Instituto de Nanociencia y Materiales de Aragón (INMA), CSIC- Universidad de Zaragoza, Zaragoza 50009, Spain*
[e.] *Instituto de Ciencia Molecular (ICMol), Universidad de Valencia, Calle Catedrático José Beltrán 2, 46980, Paterna, Spain.*
[f.] *Institute of Chemical Research of Catalonia (ICIQ), The Barcelona Institute of Science and Technology (BIST), Av. Paisos Catalans 16, 43007 Tarragona, Spain*
[g.] *ICREA, Passeig Lluís Companys 23, 08010 Barcelona, Spain.*

Table of contents

S1. X-ray powder diffraction (XRPD) spectroscopy

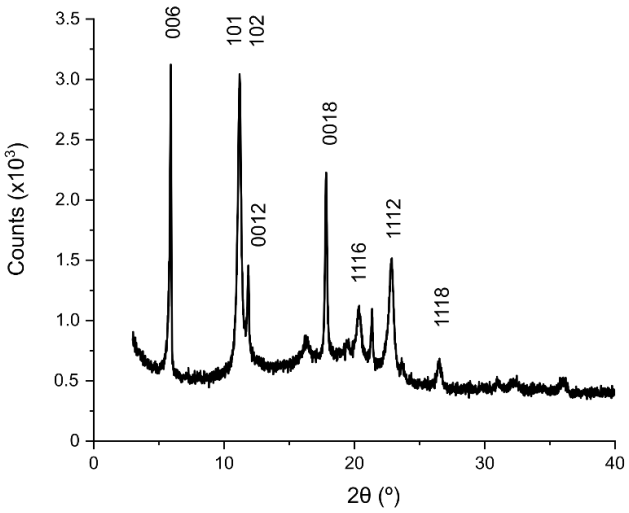

Figure S 1. *PNP[CoRh(ox)$_3$] X-ray powder diffraction (XRPD) profile indexed following Ref.* [1]

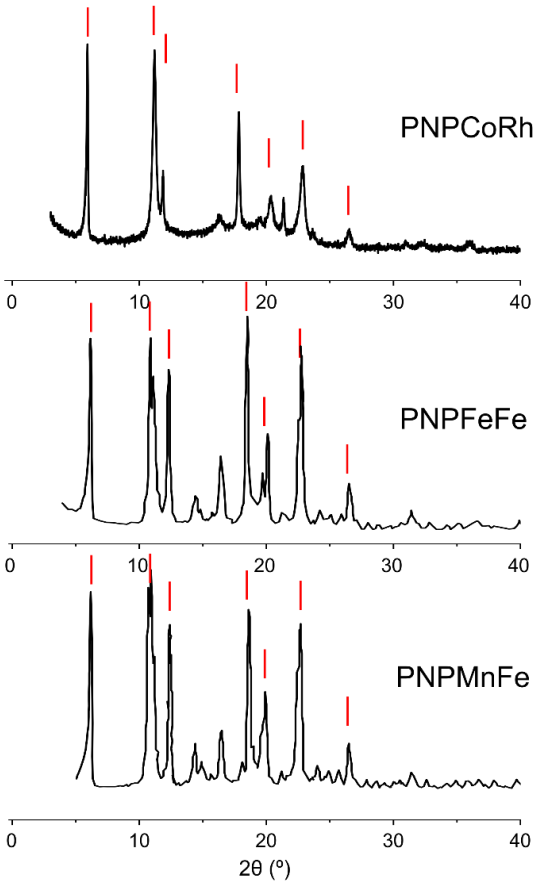

Figure S 2. *Comparison between X-ray powder diffraction patterns of PNP[CoRh(ox)$_3$] and of the isostructural PNP[FeFe(ox)$_3$] and PNP[MnFe(ox)$_3$] adapted from Ref.*[1] *The main diffraction peaks in PNPCoRh (red lines) coincide with those reported in Ref.*[1] *for structural equivalent materials with different metallic centers.*

Table S 1. *Refined unit cell parameters of PNP[FeFe (ox)$_3$] and PNP[MnFe(ox)$_3$] at room temperature reported in Ref.*[1]

Compound	Space group used for refinement	*a* (Å)	*b* (Å)	*c* (Å)	*Interlayer distance* (Å)
PNP[FeFe(ox)$_3$]	P 6(5)	9.38(1)	9.38(1)	86.6(2)	14.5
PNP[MnFe(ox)$_3$]	P 6(5)	9.41(1)	9.41(1)	87.1(2)	14.5

S2. Inductively Coupled Plasma Mass Spectrometry (ICP-MS)

The metallic proportion of the PNP[CoRh(ox)$_3$] samples is determined by inductively coupled plasma mass spectroscopy. First, the sample is atomized in a microwaves oven. Thereafter the CoRh ratio is determined in a Agilent 7900 ICP-MS. The result on two different test samples is summarized in Table S2:

Table S 2. *Co and Rh composition measured in a Agilent 7900 ICP-MS*

Sample	Co (mg/g)	Rh (mg/g)
PNP[CoRh(ox)3]- Sample 1	25.2 ± 0.4	49.4 ± 0.8
PNP[CoRh(ox)3]- Sample 2	14.8 ± 0.3	30.8 ± 0.2

Taking into account the atomic mass of Co and Rh: 58.999 g/mol and 102.9055 g/mol, the Co/Rh ratio in the material can be estimated, as summarized in Table S3. The value is very close to a 1:1 ratio expected for the PNP[CoRh(ox)$_3$] oxalate.

Table S 3*. Rh/Co ratio estimated from the ICP-MS analysis in Table S2*

Sample	Co (mmol/g)	Rh (mmol/g)	Rh/Co Ratio
PNP[CoRh(ox)$_3$]- Sample 1	0.427	0.480	1.124
PNP[CoRH(ox)$_3$]- Sample 2	0.251	0.299	1.193

The complex formula is $[Ph_3NNPh_3][CoRh(C_2O_4)_3](H_2O)_3$ with sum: $N_2O_{15}RhCoC_{42}H_{36}$. The molecular weight is m_w= 970.5910 g/mol

S3. Additional Electron Paramagnetic Resonance (EPR) spectroscopy spectra

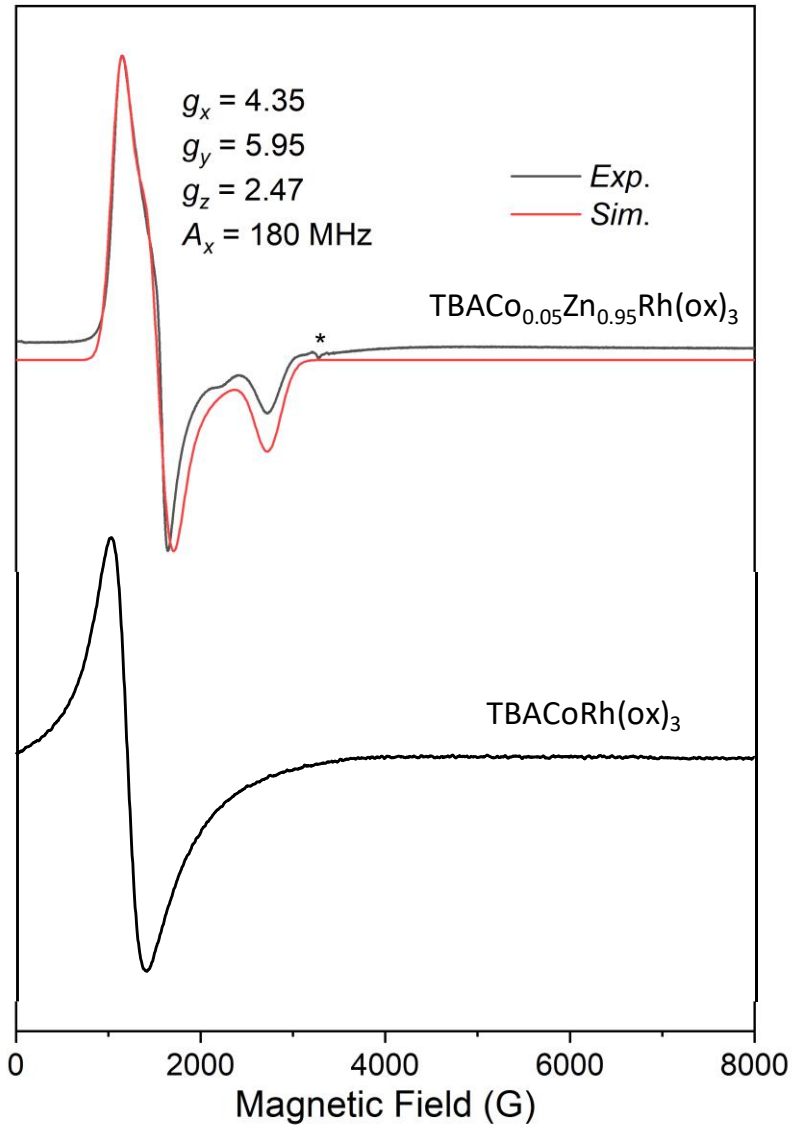

Figure S 3 *The analogous isolated [tetrabutylammonium (TBA)]CoRh(ox)$_3$ center, with an identical 2D CoRh oxalate lattice, was dissolved in a Zn (diamagnetic) matrix. The corresponding EPR spectrum can be understood from a distorted octahedral environment of Co(II). The simulation allows determining the anisotropic g values and an upper limit for the hyperfine splitting. The magnetic exchange interaction in the all-Co(II) sample causes an averaging of the g anisotropy, asymmetric shape and the apparent shift to lower fields of the signal. All the spectra were taken at 20K. An asterisk is marking a spurious signal from impurities.*

S4. Electronic level structure of Co^{2+} in [PNP]CoRh

The electronic configuration of a Co^{2+} ion is [Ar]$3d^7$. The electronic ground state according to Hund's rules is then ^4F with L = 3 and S = 3/2, resulting in $2L+1$ = 7 initially degenerated levels for the free ion, as seen in Figure S4.

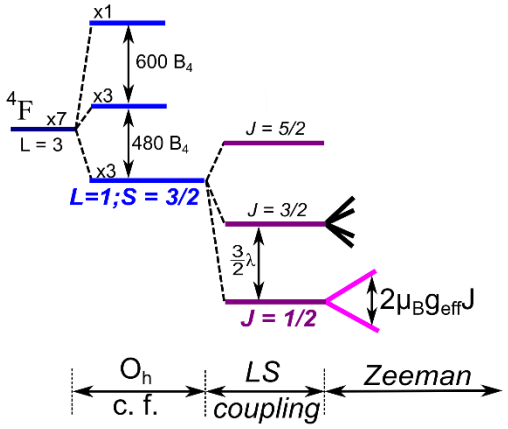

***Figure S 4**. Energy level diagram of the Co^{2+} in an octahedral field resulting from the successive application of the interaction terms in Eq. 1. The ground state can be described with an effective angular momentum J = 1/2 and g_{eff} = 4.33.* [2]

The Hamiltonian describing Co^{2+} ions in the octahedral ligand field introduced by the coordination with the oxalate ligands is:

$$\mathcal{H} = \mathcal{H}_{crys} + \mathcal{H}_{SO} + \mathcal{H}_{hyperfine} + \mathcal{H}_{Zeeman} \qquad \textit{Eq. 1}$$

where $\mathcal{H}_{crys}$ is the crystal field contribution, $\mathcal{H}_{SO}$ is the spin-orbit coupling, $\mathcal{H}_{hyperfine}$ is the hyperfine contribution due to the coupling between nuclear and electronic spins and $\mathcal{H}_{Zeeman}$ is the Zeeman contribution describing the interaction with the external magnetic field B.

The three oxalate ligands surrounding the Co^{2+} give rise to an octahedral symmetry of the form

$$\mathcal{H}_{crys} = B_4(O_4^0 + 5O_4^4) \qquad \textit{Eq. 2}$$

Where O_m^l are Stevens operators and B_4 is related to the strength of the crystal field. Assuming and intermediate ligand field, the initially degenerate levels split as seen in Figure S4. The lowest lying energy level is a degenerate orbital triplet with an effective orbital momentum $\hat{L} = 1$ and S = 3/2.

Finally the spin-orbit coupling given by $\mathcal{H}_{SO} = \lambda\vec{L}\cdot\vec{S}$ breaks the ground state degeneracy into three sets of levels with effective angular momentum $J = \pm 1/2, \pm 3/2, \pm 5/2$ as seen in Figure S4. The ground state can be described as degenerated doublet $J = \pm 1/2$ with g = 4.33.[2] Deviations from the latter value arise as a result of distortions from perfect octahedral symmetry and spin-spin interactions (see previous section).

S5. Modelling of the specific heat measurements

Schottky contribution: Fluctuation-dissipation theorem

The low temperature magnetic contribution to the specific heat (c_m), known as Schottky contribution is calculated by using the fluctuation-dissipation theorem given by:

$$\frac{c_m}{R} = \frac{\langle U^2 \rangle - \langle U \rangle^2}{T^2} \qquad \textit{Eq. 3}$$

Where R is the gas constant and U is the internal magnetic energy of the system:

$$U = N_A \frac{\sum_i E_i e^{-\frac{E_i}{k_B T}}}{Z} \qquad \textit{Eq. 4}$$

where N_A is the Avogadro number, Z is the partition function and E_i are the magnetic energy levels obtained from the diagonalization of the spin Hamiltonian of each isolated Co^{2+} ion.

Heisenberg model for a J = 1/2 system.

For B = 0 and sufficiently low temperatures, the specific heat given by Eqs. 3 and 4 nearly vanishes, as the two levels associated with the J = 1/2 ground state are degenerate and hyperfine interactions are too weak to give rise to a sizeable contribution. The specific heat high-temperature tail observed experimentally (see Figure 3b in the main text), requires then to go beyond the picture of isolated spins. Spin-spin interactions can be approximately modeled by using a J = 1/2 Heisenberg model. The high-T approximation for the specific heat is then:[2]

$$\frac{c}{R} = \frac{1}{2}\left(\frac{J(J+1)}{3K_B}\right)^2 Z \frac{3J_{eff}^2}{T^2} \qquad \textit{Eq. 5}$$

Where Z = 6 is the number of nearest neighbors, J = 1/2 is the effective angular momentum and J_{eff} is the effective spin-spin coupling strength. Fitting the experimental data measured at B = 0 using Eq. 5 gives J_{eff} = 0.2 K (see Fig. 3b in the main text).

S6. Entropy

The entropy content S_m of a magnetic system is given by:

$$S_m = Rln(2J+1) \qquad \textit{Eq. 6}$$

where *J* is the effective spin. The magnetic entropy can be determined from the experimental specific heat as:

$$\frac{S_m(T)}{R} = \int_0^T \frac{c_m}{T} dT \qquad \textit{Eq. 7}$$

Figure S5 shows S_m as a function of temperature for B = 1 T obtained from the c_m data shown in Figure 2b of the main text. A saturation value of $S_m \approx R\ln 2 = 0.69R$ is found which, according to Eq. 6, corresponds to J = 1/2. In addition, this shows that the J = 1/2 ground state is the only populated level below 10 K.

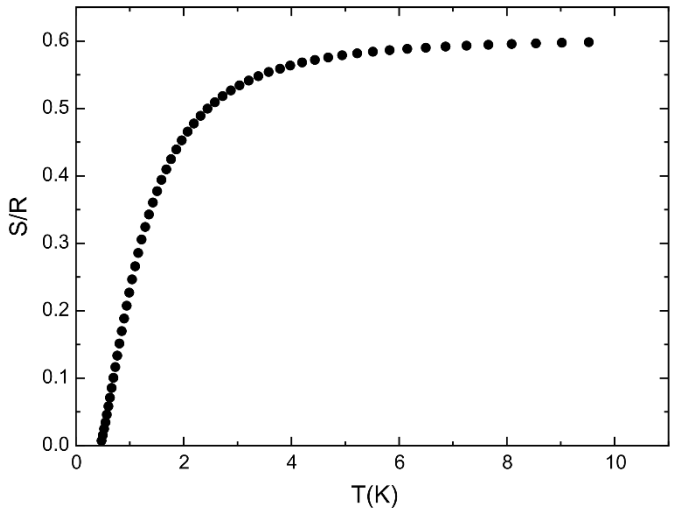

Figure S 5. *Magnetic entropy S_m calculated by using Eq. 7 and the specific heat at B = 1 T in the main text. The saturation value is close to 0.69, consistent with a J = 1/2 ground state. The entropy shows that the ground state is the only populated level in this range of temperatures*

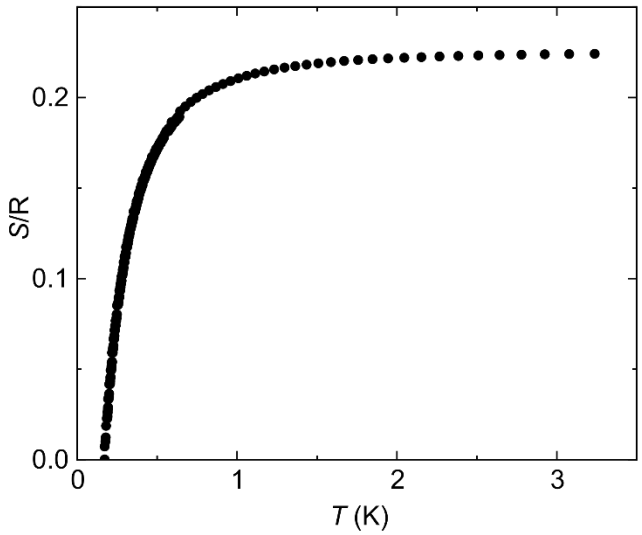

***Figure S 6**. Magnetic entropy S_m calculated by using Eq. 7 and the specific heat at B = 0 T in the main text.*

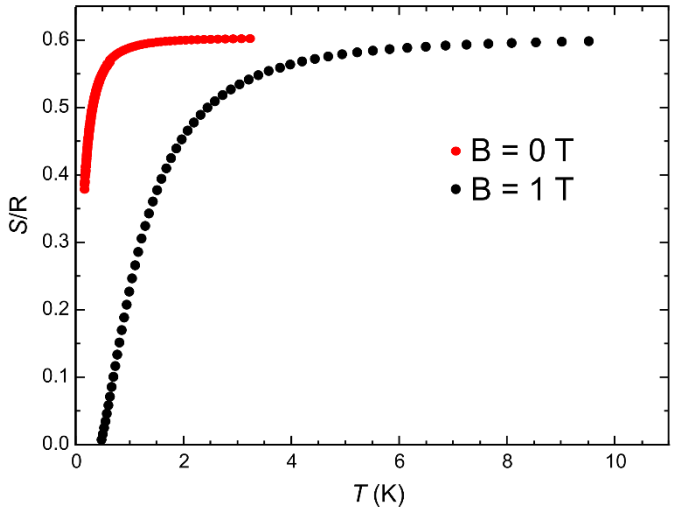

***Figure S 7**. Magnetic entropy at 0 T and 1T from Figures S5 and S6. Entropy at 0T has been scaled for comparison.*

S7. Modelling of the magnetic susceptibility measurements

Figure 4a in the main manuscript shows that $\chi'T$ continuously drops with decreasing temperature. This occurs mainly as a consequence of the depopulation of excited electronic states.

The temperature dependence of χ can be described by considering the two lowest doublets separated by the energy Δ:[3]

$$\chi = \frac{N}{k_B(T-T_0)}\left\{C_0 + C_1\left(\frac{2k_BT}{\Delta}\right)tanh\left(\frac{\Delta}{2k_B}\right) + C_2\,tanh\left(\frac{\Delta}{2k_BT}\right)\right\} + \chi_0 \qquad \textit{Eq. 8}$$

Where N is the number of paramagnetic entities, k_B is the Boltzmann constant, the C_0, C_1 and C_2 quantities depend on the electronic wave function of the two Kramers doublets involved, and χ_0 accounts for diamagnetic and other temperature independent contributions to the magnetic susceptibility. T_0 accounts for the magnetic interactions with the neighboring atoms, and plays the role of an effective Weiss temperature.

The fit to the experimental χT in Figure 4a is obtained with the values summarized in Table S4. The large Δ value confirms that the system can be simplified to a single $J = 1/2$ doublet below 15 K. Moreover, the curve can only be fitted by introducing a finite T_0 value, accounting for interactions.

Note that C_2 is negligible small within the error. For low enough temperatures, that that is $T << \Delta$, the susceptibility can be approximated to $\chi = N(C_0+C_2)/kB\ (T-T_0)+\chi_0$, as shown in ref[1]. A negligible small C_2 value would imply a $\chi \approx N(C_0)/kB\ (T-T_0)+\chi_0$, that is, the Curie law for an isolated doublet. In other words the smaller C_2 the more the system behaves as an isolated doublet at low temperatures.

Table S 4*. Fitting values for the parameters in Eq. 8.*

Parameter	**Fitting value**
Δ	366 K
C_0	1.68 emuK/mol
C_1	8.23 emuK/mol
C_2	0 emuK/mol
X_0	-0.031 emu/mol
T_0	-0.38 K

S8. Bibliography

1 C. J. Nuttall, PhD Thesis:Bimetallic tris-oxalate magnets: Synthesis, structure and properties. ProQuest U642291. University of London, 1998.

2 A. Abragam and B. Bleaney, *Electron Paramagnetic Resonance of Transition Ions (Oxford Classic Texts in the Physical Sciences)*, Oxford University Press, USA, 2012.

3 E. Bartolomé, P. J. Alonso, A. Arauzo, J. Luzón, J. Bartolomé, C. Racles and C. Turta, *Dalt. Trans.*, 2012, **41**, 10382–10389.